Spectral dependence of the scattering coefficient in case 1 and case 2 waters

Richard W. Gould, Jr., Robert A. Arnone, and Paul M. Martinolich

An approximate linear relationship between the scattering coefficient and the wavelength of light in the visible is found in case 1 and case 2 waters. From this relationship, we estimate scattering at an unknown wavelength from scattering at a single measured wavelength. This approximation is based on measurements in a 1.5-m-thick surface layer collected with an AC9 instrument at 63 stations in the Arabian Sea, northern Gulf of Mexico, and coastal North Carolina. The light-scattering coefficient at 412 nm ranged from 0.2 to 15.1 m^{-1} in these waters, and the absorption coefficient at 412 nm ranged from 0.2 to 4.0 m^{-1}. A separate data set for 100 stations from Oceanside, California, and Chesapeake Bay, Virginia, was used to validate the relationship. Although the Oceanside waters were considerably different from the developmental data set (based on absorption-to-scattering ratios and single-scattering albedos), the average error between modeled and measured scattering values was 6.0% for the entire test data set over all wavelengths (without regard to sign). The slope of the spectral scattering relationship decreases progressively from high-scattering, turbid waters dominated by suspended sediments to lower-scattering, clear waters dominated by phytoplankton.

OCIS codes: 010.4450, 290.5820, 290.5850, 290.1350.

1. Introduction

The scattering coefficient b is an inherent optical property directly related to remote-sensing measurements of ocean color. The importance of b to remote-sensing reflectance (R_{rs}) is linked to the backscattering coefficient b_b, which represents the backward component of b (i.e., scattering integrated over the angles from 90° to 180°). Irradiance reflectance R, the ratio of upwelling irradiance (E_u) to downwelling irradiance (E_d) just beneath the water surface, is related to the absorption a and backscattering coefficients of the water through the equation

$$R = f b_b / a. \quad (1)$$

The f coefficient depends on solar zenith angle, sea state, and shape of the scattering phase function.[1] A value of 0.33 was calculated for the f coefficient for a zenith Sun and a flat sea surface.[2] In coastal waters, scattering by high concentrations of inorganic particles strongly influences the submarine light field to an even greater extent than absorption processes in some cases; thus b_b is a major component of the reflectance equation.

Remote-sensing reflectance, the ratio of water-leaving radiance L_w to downwelling irradiance, is related to R through an irradiance–radiance conversion Q and an air–sea interface transfer function.[1,3] Therefore inversion models are being developed to estimate a and b_b from in-water and above-water reflectance measurements through a variety of techniques.[4–8] To achieve this goal, predictive relationships between a and b_b and the wavelength of light λ are required. Power functions of the form b or $b_b \sim \lambda^n$ have been proposed to describe the shapes of scattering and backscattering spectra. The exponent n is typically assigned a value of -1, but values from 0 to -4 have been applied to spectra from eukaryotic and prokaryotic taxa representing a wide variety of size classes (bacteria, cyanobacteria, viruses, flagellates, ciliates, and several phytoplankton species).[7,9–15] The larger species examined showed comparatively flatter spectral scattering shapes, with pigment absorption effects superimposed on the phytoplankton spectra.[11,13] Little research has been done in coastal waters that are dominated by scattering from suspended sediments.

R. W. Gould, Jr., and R. A. Arnone are with the Remote Sensing Applications Branch, Naval Research Laboratory, Code 7343, Stennis Space Center, Mississippi 39529. P. M. Martinolich is with Neptune Sciences, Incorporated, 150 Cleveland Avenue, Slidell, Louisiana 70458. The e-mail address for R. W. Gould is gould@csips.nrlssc.navy.mil.

Received 24 July 1998; revised manuscript received 4 January 1999.

0003-6935/99/122377-07$15.00/0

Table 1. Stations Comprising the Model Development and Validation Data Sets

Location	Date	Data Set Type	Number of Stations
Arabian Sea	September–October 1995	Development	24 (case 1)
Mississippi Bight	March, June, July 1996	Development	21 (case 1 and 2)
Coastal North Carolina	March 1996	Development	18 (case 2)
Oceanside, California	October 1995	Validation	31 (case 1)
Chesapeake Bay, Virginia	September 1996	Validation	69 (case 1 and 2)

To facilitate ongoing efforts to develop and validate reflectance inversion models that estimate a and b_b from R_{rs}, independent measurements of a and b_b are required for error analysis. Light attenuation c and absorption coefficients a in seawater (and thus b values, by difference) are readily measured with a variety of techniques and instruments that are in fairly widespread and routine use.[16] Because few measurements of b_b have been collected to date, however, we present a conversion to b_b from measurements of b based on Petzold[17] data.

Our objective is to examine the spectral dependence of the scattering coefficient and develop a model to estimate scattering at any wavelength from scattering at a single, measured reference wavelength. We use an approach similar to Austin and Petzold[18] who estimated the spectral dependence of the diffuse attenuation coefficient K_d in clear oceanic waters. They found linear relationships between wavelengths and developed a model to estimate $K_d(\lambda)$ from a known K_d value at a reference wavelength. We present a simple linear regression model to estimate spectral scattering based on measurements from clear case 1 waters as well as turbid case 2 waters. We validate the scattering model using an independent data set and examine errors between model results and measurements.

2. Methods

Depth profiles of light absorption $a(\lambda)$ and attenuation $c(\lambda)$ were collected at nine wavelengths with an AC9 meter in clear, open-ocean case 1 waters of the Arabian Sea and in turbid, coastal case 2 waters of the Mississippi Bight (northern Gulf of Mexico) and Onslow Bay (Camp Lejeune, North Carolina).[19] Measurement wavelengths were 412, 440, 488, 510, 532, 555, 650, 676, and 715 nm. A total of 63 stations formed the experimental data set used to derive the scattering relationship presented below, with approximately two thirds of the stations representing case 2 waters (Table 1). Only surface measurements, averaged over the top 1.5 m of the water column, were used.

A temperature correction was applied to the 715-nm absorption channel,[19] and a scatter correction was applied to all absorption channels.[20] Because the AC9 instrument is calibrated in pure water, absorption values for pure water[21] were added back into the a and c values to yield total absorption and attenuation. The light-scattering coefficient was calculated as follows:

$$b(\lambda) = c(\lambda) - a(\lambda). \quad (2)$$

The scattering coefficient is comprised of scattering components that are due to pure water b_w and particulates b_p. The b_w component is small at visible wavelengths,[22] leaving b_p as the major component.

3. Results

We selected the 555-nm channel as the reference channel because of the low absorption at that wavelength in coastal waters and because of its location near the middle of the wavelength range of the AC9 (thereby minimizing errors that could result by using too large a wavelength interval in the regression analyses). For each of the remaining eight AC9 wavelengths we fitted a linear function:

$$b(\lambda) = M(\lambda)b(555) + I. \quad (3)$$

In each case, R^2 values exceeded 0.99 over a range of the scattering coefficient b at 555-nm [$b(555)$] values up to 14 m^{-1} (Fig. 1). The regression slopes show a regular decrease with increasing wavelength from 412 to 715 nm. Regression slope, intercept, and R^2 values are indicated in Table 2 for each wavelength. The intercepts for all these regressions deviate slightly from zero, indicating errors in measurement

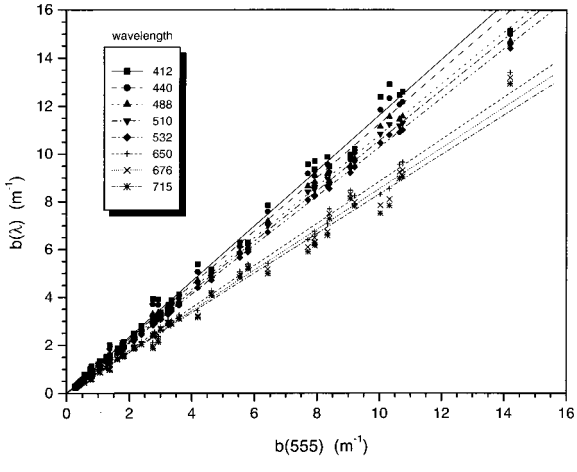

Fig. 1. Wavelength dependence of scattering, $b(\lambda)$ versus b(555) for λ = 412, 440, 488, 510, 532, 650, 676, and 715 nm (AC9-derived values). The curves represent least-squares linear regressions. Slopes, intercepts, and R^2 values are listed in Table 2.

Table 2. Spectral b Least-Squares Linear Regression Results[a]

Wavelength	Slope M (standard error)	Intercept I (standard error)	R^2
412	1.16031 (0.01187)	0.00781 (0.05602)	0.994
440	1.12374 (0.00904)	0.01284 (0.04266)	0.996
488	1.07436 (0.00549)	0.02856 (0.02589)	0.998
510	1.05478 (0.00426)	0.00497 (0.02012)	0.999
532	1.02606 (0.00223)	0.01380 (0.01053)	0.999
650	0.88219 (0.00779)	0.02074 (0.03676)	0.995
676	0.85308 (0.00945)	0.00534 (0.04462)	0.992
715	0.82819 (0.01013)	0.02969 (0.04783)	0.991

[a] $b(\lambda) = M \times b(555) + I$.

or instrument calibration (see Section 4). Because the intercepts should be zero, and because the errors associated with a different data set would vary from those associated with this set (thus varying the intercept values), we neglect the intercepts during further development of our scattering model. $M(\lambda)$ is a linear function of the wavelength of light (Fig. 2):

$$M(\lambda) = \mathrm{m}\lambda + i, \tag{4}$$

with m = −0.00113, i = 1.62517, and R^2 = 0.997. Therefore we can estimate the slope $M(\lambda)$ based solely on wavelength, and we can derive $b(\lambda)$ at any wavelength [within the range for which Eqs. (3) and (4) were established] if we know b at a single reference wavelength (λ_r):

$$b(\lambda_r) = M(\lambda_r)b(555), \quad b(\lambda) = M(\lambda)b(555), \tag{5}$$

$$M(\lambda_r) = \mathrm{m}\lambda_r + i, \quad M(\lambda) = \mathrm{m}\lambda + i. \tag{6}$$

Inserting Eqs. (6) into corresponding Eqs. (5),

$$b(\lambda_r) = (\mathrm{m}\lambda_r + i)b(555), \tag{7}$$

$$b(\lambda) = (\mathrm{m}\lambda + i)b(555). \tag{8}$$

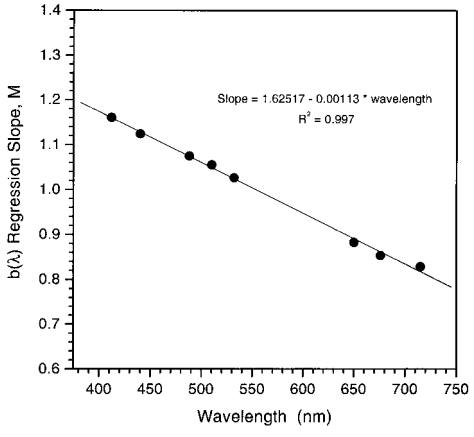

Fig. 2. Regression slope versus wavelength. The slope values M are from the regression analyses of the $b(\lambda)$ versus b(555) data shown in Fig. 1. The solid line represents the least-squares regression fit to the data, with slope, intercept, and R^2 values indicated.

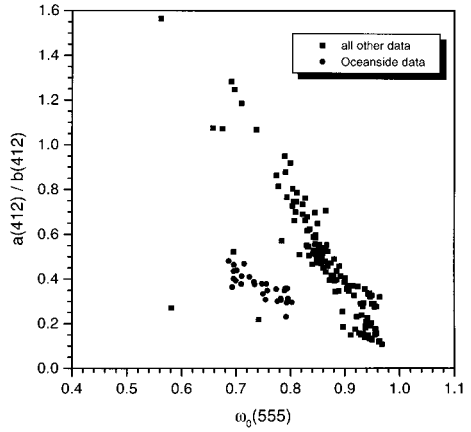

Fig. 3. $a(412)/b(412)$ ratio versus $\omega_0 555$. Circles indicate stations from Oceanside, California; squares indicate stations from all other locations (including both model development and validation data sets).

Solving both Eqs. (7) and (8) for $b(555)$ and setting equal,

$$b(\lambda_r)/(\mathrm{m}\lambda_r + i) = b(\lambda)/(\mathrm{m}\lambda + i). \tag{9}$$

Solving Eq. 9 for b at the unknown wavelength λ,

$$b(\lambda) = b(\lambda_r)(\mathrm{m}\lambda + i)/(\mathrm{m}\lambda_r + i). \tag{10}$$

Thus we can calculate b at any wavelength if we know the b value at a single reference wavelength.

To test our scattering model, we used an independent AC9 data set of 100 stations collected in coastal waters off Oceanside, California, in October 1995 and off Chesapeake Bay in September 1996 (Table 1). The test data set was processed in the same way as the developmental data set (the AC9 instruments were different, however). The wavelength set for the Chesapeake Bay stations was slightly different from the other locations; a channel at 630 nm replaced the 532-nm channel.

The $a(412)/b(412)$ ratio (where the absorption coefficient a is measured at 412 nm) and the single-scattering albedo ω_0 at 555 nm [$\omega_0(555) = b(555)/c(555)$] indicate that the Oceanside waters differed considerably from most of the other samples comprising the developmental and validation data sets (Fig. 3). The lower $a(412)/b(412)$ ratios suggest lower levels of absorption by dissolved organic matter at the Oceanside stations, as dissolved organic matter absorbs strongly at 412 nm, but the lower $\omega_0(555)$ values also indicate that Oceanside was still a more absorption-dominated regime than the other areas.

Pigment data were collected in conjunction with the AC9 data for the Chesapeake Bay samples. Thus we can apply Morel's model[10] to estimate $b(550)$ from pigment concentration [$b(550) = 0.30\ C^{0.62}$, where C is the sum of the chlorophyll and phaeophytin concentrations] and compare the results to the AC9-derived $b(555)$ values (Fig. 4). For the case 1 water samples (the regime where the Morel model was developed), measured and modeled values agree

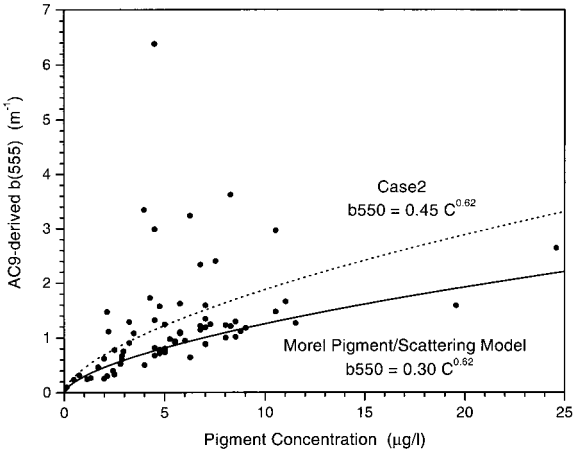

Fig. 4. AC9-derived $b(555)$ versus pigment concentration (sum of chlorophyll and phaeophytin) for Chesapeake Bay stations. Solid curve represents the Morel[11] model to estimate $b(550)$ from pigments; dotted curve represents the Morel[11] limit for case 1 waters (i.e., points on or above the dotted curve are from case 2 waters).

quite well. For case 2 waters (points above the dotted curve in Fig. 4), Morel's model significantly underestimates the AC9-measured $b(555)$ values because of the high concentrations of suspended sediments that contribute to the scattering signal but not the pigment levels.

With Eq. (10) we can estimate spectral b if we know b at a single wavelength. However, to facilitate comparisons with inversion model estimates of b_b, a conversion from b to b_b would be beneficial. Petzold[17] measured the volume-scattering function at a variety of locations (including turbid San Diego Harbor) over a wide range of scattering angles (0.085° to 170°) and calculated b and b_b values, and these volume-scattering functions have been widely cited. Therefore we used Petzold's data[17] to derive a least-squares linear regression between b_b and b (Fig. 5). We believe that this relationship is applicable over a wide wavelength range because the spectral response of the instruments used by Petzold was quite broad

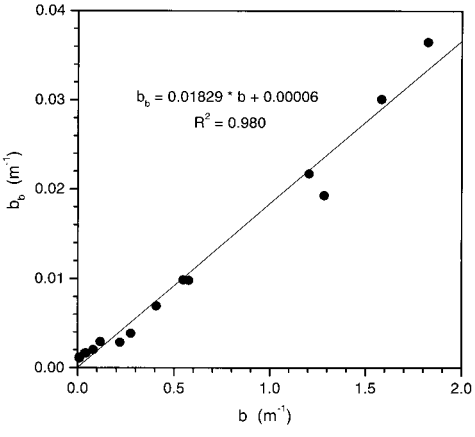

Fig. 5. Backscattering versus scattering (data from Petzold[17]). The solid line represents the least-squares regression fit to the data, with slope, intercept, and R^2 values indicated.

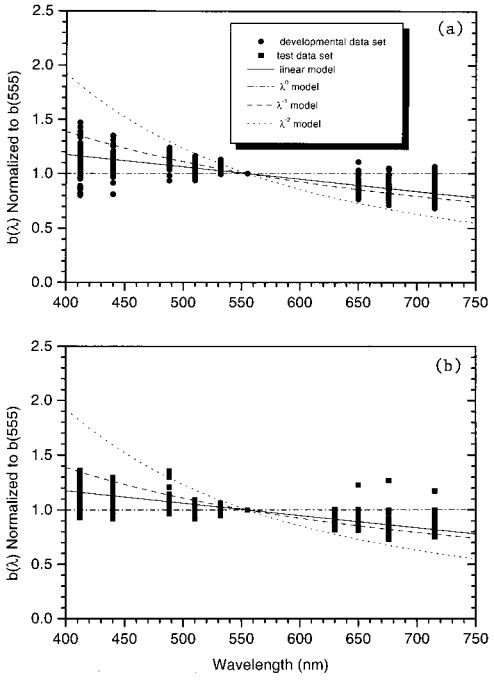

Fig. 6. $b(\lambda)$ normalized to $b(555)$ versus wavelength. (a) Developmental data set (circles). (b) Test data set (squares). Linear and power model ($n = 0, -1, -2$) spectra are indicated for comparison with the data distributions.

(centered around 515 nm but extending from 400 to 600 nm; Fig. 3 in Petzold[17]). We recognize that the parameters of such a regression may vary seasonally and regionally based on particle size, shape, and composition (i.e., index of refraction).

We can compare our linear approximation for scattering, $b \sim \lambda$, with power function approximations that have been proposed to describe the shape of scattering spectra, $b \sim \lambda^n$. In Fig. 6, we plot spectral scattering values from both the developmental and the test data sets, normalized to 555 nm, with the linear and power functions overlaid ($n = 0, -1, -2$). Note that there is quite a large range in the normalized b values at any given wavelength, particularly at the 412 and 440 wavelengths [Fig. 6(a)]. So although the linear model presented here provides a good fit on average, there can be large deviations when the model is applied to individual stations.

To validate our model, we selected the 555-nm channel as the reference, calculated b at 412, 440, 488, 510, 532, 630, 650, and 676 nm using Eq. (10) and the validation data set, and evaluated the model's performance by calculating differences between measured and model-estimated b values. Errors between modeled and measured scattering values were calculated as follows (Fig. 7):

$$\text{percent error} = 100\,[\text{modeled } b(\lambda) - \text{measured } b(\lambda)]/\text{measured } b(\lambda). \quad (11)$$

The range of measured $b(412)$ values at Oceanside was quite small (0.18–0.55 m^{-1}) and at the extreme

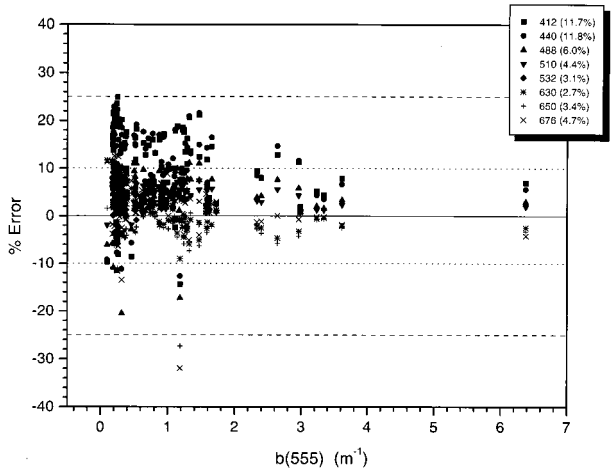

Fig. 7. Percent error between modeled and AC9-derived $b(\lambda)$ values versus $b(555)$. Model results are from the validation data set (Oceanside and Chesapeake Bay stations). Dotted lines indicate $\pm 10\%$ error; dashed lines indicate $\pm 25\%$ error. In the legend, the values in parentheses indicate the average percent error for each wavelength, without regard to the sign of the error (for example, the average of a 10% and a -10% error is 10%, not 0).

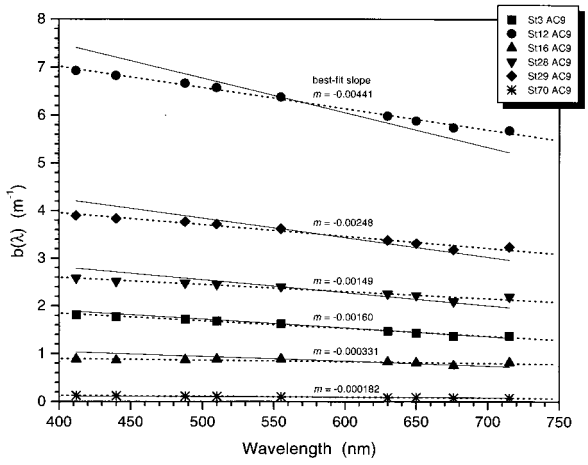

Fig. 8. Scattering coefficient versus wavelength. Selected stations are from the Chesapeake Bay region (validation data set) covering a wide range of scattering values. Note the decrease in the spectral slope as the scattering magnitude decreases. Solid lines are model results; dotted lines are least-squares regression fits to the AC9-derived values. Spectral slope values m are indicated for the regression lines.

lower range of the data set used for model development (see Fig. 1). Values of $b(412)$ from the Chesapeake Bay samples covered a wider range (0.13–6.9 m^{-1}).

Although some data from the validation set differed considerably from the developmental data set, modeled scattering values were nearly all within 25% of measured values and were generally within 10% for wavelengths greater than 440 nm (Fig. 7). Errors tend to decrease with increasing $b(555)$ values. The model systematically overestimated b at wavelengths less than the 555-nm reference wavelength. Figure 8 shows data from the Chesapeake Bay region for six stations covering a wide range of scattering levels. The overestimation of scattering by the model at shorter wavelengths and slight underestimation at longer wavelengths are evident.

There is a gradual decrease in the spectral scattering slope m as $b(555)$ values decrease (Fig. 8). The decrease in the slopes of the measured scattering spectra (dashed lines) is mimicked by a decrease in the slopes of the modeled spectra (solid lines), although the magnitudes of any two corresponding measured and modeled slopes are not quite equal. Using any two wavelengths λ and λ_r, we can define m as

$$m \equiv [b(\lambda) - b(\lambda_r)]/(\lambda - \lambda_r). \quad (12)$$

Coupled with Eq. (10), the previously calculated values of m and i (-0.00113 and 1.62517, respectively), and a reference wavelength λ_r of 555 nm, we can estimate m from $b(555)$:

$$m = -0.00113\, b(555). \quad (13)$$

Thus the spectral scattering slope is a function of $b(555)$. At low $b(555)$ values, the slope is nearly zero (station 70, Fig. 8).

4. Discussion

This spectral b model was developed with surface AC9 measurements from 63 stations representing three disparate environments including both case 1 and case 2 waters (Arabian Sea, northern Gulf of Mexico, and coastal North Carolina), and it was tested using 100 stations from quite different areas also representing case 1 and case 2 waters (coastal California and Chesapeake Bay). Differences between predicted and measured values were low when averaged over all wavelengths combined, suggesting that this universal model should be valid over a wide range of coastal and oceanic environments. In the low-scattering regime where the model was tested, however (Oceanside, California), average errors for individual wavelengths in the blue part of the spectrum (412, 440 nm) exceeded 15%.

Barnard *et al.*[23] examined spectral relationships for oceanic inherent optical properties, including a, b, and c. Whereas their data set included all depths from 77 vertical profiles, our data set included surface b values from 63 stations. However, in only six of their 1914 samples did $b(488)$ exceed 4.0 m^{-1} (with a maximum of 6.6 m^{-1}), whereas 17 of our samples exceeded 4.0 m^{-1} (with a maximum of 14.1 m^{-1}). Thus our data set may be more representative of turbid water. Because the linear regressions between $b(555)$ and $b(\lambda)$ are strongly influenced by the high values (Fig. 1), our intercepts deviate from zero and are slightly larger than those of Barnard *et al.*[23] at several wavelengths. Similarly, when Barnard *et al.*[23] split their data set into upper and lower order of magnitude subsets, their regression intercepts were

larger for the upper-order data sets. They suggested that the nonzero intercepts (that exceed the AC9 measurement accuracy of approximately $\pm 0.005\ m^{-1}$ for individual a and c measurements or $\pm 0.007\ m^{-1}$ for values derived from two measurements, such as b) may be due to a background concentration of detrital and dissolved absorption that does not covary with the particulate absorption.

Our scattering regression slopes decrease linearly with wavelength (Fig. 2), whereas those of Barnard *et al.*[23] are nearly constant and equal to 1.0 (i.e., a flat scattering spectrum; their Fig. 5). However, we do observe a flattening of the scattering spectra at low scattering values in both our data and our model results. Barnard *et al.*[23] describe linear inherent optical property relationships and interpret their variability. We present similar analyses for scattering only and extend the results a step further to provide an estimate of spectral $b(\lambda)$ from a single b measurement at another wavelength.

The b_b/b ratio (backscattering efficiency) of 0.0183 from Fig. 5 is of the same order of magnitude as that derived experimentally by Sydor and Arnone[24] (0.0125) from measurements of R_{rs}, a, and b, and as the value of 0.021 provided by Morel.[10] The backscattering efficiency of phytoplankton is much lower than for detrital particles. Bricaud *et al.*[11] reported species-specific values ranging from 0.0001 to 0.0015 for culture samples. Coccolithophorids are an exception, however; cells and detached coccoliths can represent a significant backscattering signal in open-ocean regions during bloom conditions.[25] Only recent developments in optical instrumentation have enabled direct *in situ* measurement of b_b.[26]

Theory shows that the spectral behavior of b and b_b coefficients may not be the same.[27] For a given taxon, measured b and b_b spectra in some cases exhibit fairly similar shapes in general and in other cases dissimilar shapes.[11,12,14,15] For a variety of microbial particles, there is an increase in the backscattering ratio b/b_b with increasing wavelength.[13] This spectral dependence is related to the particle size relative to the wavelength of light and the greater effective backscattering by smaller particles, so a similar spectral dependence could be expected for detrital particles. However, because the relationship in Fig. 5 was developed over a broad wavelength band and the presence of a wide variety of particle types and sizes in any given sample, the regression slope may represent a wavelength-independent average backscattering ratio. More research is required with sediments to compare b and b_b spectra over a wide variety of size classes and refractive indices and to assess spectral dependence in the b/b_b relationship for turbid waters.

The slope of the b versus wavelength relationship varies depending on the magnitude of the scattering and on the composition of the scatterers. In areas with high b values dominated by suspended sediments, such as the coastal North Carolina, Chesapeake Bay, and Mississippi sites, there is a relatively steep negative slope to the b versus wavelength relationship [i.e., $b(\lambda)$ decreases with increasing wavelength; see stations 12 and 29 in Fig. 8]. In clear areas with low b values dominated by phytoplankton, such as the Arabian Sea and Oceanside sites, the shape is flat or nearly so. From Eq. (13) it is apparent that the regional differences in the slope are a result of the regional differences in the magnitude of $b(555)$. The differences are not accounted for by determining slopes over a narrow range of scattering coefficients because the model regression parameters were determined using all the scattering data over a wide range of values.

This gradual decrease in the slope of the b versus wavelength relationship from turbid to clear waters is supported by other field studies. Sydor and Arnone[24] showed a decrease in the slope proceeding from river, bay, and near-shore stations to offshore Gulf of Mexico waters (their Fig. 3). Whitlock *et al.*[28] observed a similar linear decrease in scattering with increasing wavelength at three of their four stations in turbid river waters. They found a relationship between the scattering level and the combined particulate mixture of chlorophyll and suspended solids. Gordon and Morel[9] and Morel[10] also related scattering and backscattering coefficients to pigment concentration. At the Chesapeake Bay study site where we had both pigment and AC9 scattering measurements, the Morel[10] pigment-to-scattering model worked well for the case 1 water samples but underestimated scattering values at the turbid case 2 sites.

5. Conclusion

The linear spectral scattering model presented here can be used to derive b at any wavelength within the 400–700-nm range if b is known at a single wavelength for both case 1 and case 2 waters. The model development approach we used is similar to that of Austin and Petzold[19] for the spectral diffuse attenuation coefficient. The model predictions agreed with independent experimental data to better than $\pm 6\%$ over all wavelengths examined (without regard to sign); however, the model slightly overestimates scattering at wavelengths less than 555 nm. This spectral b relationship can be incorporated into inversion models that estimate a and b_b from reflectance measurements.

The slope of the scattering versus wavelength relationship determined from AC9 data decreased progressively from -0.0044 in turbid waters dominated by suspended sediments [$b(555) = 6.4\ m^{-1}$] to -0.00018 in clear waters dominated by phytoplankton [$b(555) = 0.1\ m^{-1}$], but the relationship remained linear. As the suspended sediment contribution to total scattering decreases and the contribution by phytoplankton increases, the shape of the spectral scattering relationship flattens.

We thank Greg Terrie, Chris Wood, and Sherwin Ladner for assistance with data collection and processing. Scott Pegau provided the Oceanside AC9 data set. Two anonymous reviewers improved the manuscript content and style. This research was

supported by the Littoral Optical Environment PE62435, Arabian Sea/Forced Upper Ocean Dynamics 0601153n, and Spectral Signatures of the Coastal Zone PE601153n programs at the Naval Research Laboratory.

References

1. A. Morel and B. Gentili, "Diffuse reflectance of oceanic waters. III. Implication of bidirectionality for the remote-sensing problem," Appl. Opt. **35,** 4850–4862 (1996).
2. A. Morel and L. Prieur, "Analysis of variations in ocean color," Limnol. Oceanogr. **22,** 709–722 (1977).
3. Z. P. Lee, K. L. Carder, S. K. Hawes, R. G. Steward, T. G. Peacock, and C. O. Davis, "Model for the interpretation of hyperspectral remote-sensing reflectance," Appl. Opt. **33,** 5721–5732 (1994).
4. S. A. Garver and D. A. Siegel, "Inherent optical property inversion of ocean color spectra and its biogeochemical interpretation. 1. Time series from the Sargasso Sea," J. Geophys. Res. **102,** 18,607–18,625 (1997).
5. H. R. Gordon and G. C. Boynton, "Radiance–irradiance inversion algorithm for estimating the absorption and backscattering coefficients of natural waters: homogeneous waters," Appl. Opt. **36,** 2636–2641 (1997).
6. Z. P. Lee, K. L. Carder, T. G. Peacock, C. O. Davis, and J. L. Mueller, "Method to derive ocean absorption coefficients from remote-sensing reflectance," Appl. Opt. **35,** 453–462 (1996).
7. C. S. Roesler and M. J. Perry, "*In situ* phytoplankton absorption, fluorescence emission, and particulate backscattering spectra determined from reflectance," J. Geophys. Res. **100,** 13,279–13,294 (1995).
8. M. Sydor, R. A. Arnone, R. W. Gould, Jr., G. E. Terrie, S. D. Ladner, and C. G. Wood, "Remote sensing technique for determination of volume absorption coefficient of turbid water," Appl. Opt. **37,** 4944–4950 (1998).
9. H. R. Gordon and A. Morel, *Remote Assessment of Ocean Color for Interpretation of Satellite Visible Imagery: A Review* (Springer-Verlag, New York, 1983).
10. A. Morel, "Optical modeling of the upper ocean in relation to its biogenous matter content (case I waters)," J. Geophys. Res. **93,** 10,749–10,768 (1988).
11. A. Bricaud, A. Morel, and L. Prieur, "Optical efficiency factors of some phytoplankters," Limnol. Oceanogr. **28,** 816–832 (1983).
12. D. Stramski and D. A. Kiefer, "Light scattering by microorganisms in the open ocean," Prog. Oceanogr. **28,** 343–383 (1991).
13. D. Stramski and C. D. Mobley, "Effects of microbial particles on oceanic optics: a database of single-particle optical properties," Limnol. Oceanogr. **42,** 538–549 (1997).
14. A. Morel and Y.-H. Ahn, "Optical efficiency factors for free-living marine bacteria: influence of bacterioplankton upon the optical properties and particulate organic carbon in oceanic waters," J. Mar. Res. **48,** 145–175 (1990).
15. A. Morel and Y.-H. Ahn, "Optics of heterotrophic nanoflagellates and ciliates: a tentative assessment of their scattering role in oceanic waters compared to those of bacterial and algal cells," J. Mar. Res. **49,** 177–202 (1991).
16. W. S. Pegau, J. S. Cleveland, W. Doss, C. D. Kennedy, R. A. Maffione, J. L. Mueller, R. Stone, C. C. Trees, A. D. Weidemann, W. H. Wells, and J. R. V. Zaneveld," A comparison of methods for the measurement of the absorption coefficient in natural waters," J. Geophys. Res. **100,** 13,201–13,220 (1995).
17. T. J. Petzold, "Volume scattering functions for selected ocean waters," Scripps Institution of Oceanography Ref. 72–78, 79 pp. (1972).
18. R. W. Austin and T. J. Petzold, "Spectral dependence of the diffuse attenuation coefficient of light in ocean waters," in *Ocean Optics VII*, M. A. Blizzard, ed., Proc. SPIE **489,** 168–178 (1984).
19. WETLabs, Inc., "AC9 Protocol Manual," www.wetlabs.com (1998).
20. J. R. V. Zaneveld, J. C. Kitchen, and C. Moore, "The scattering error correction of reflecting-tube absorption meters," in *Ocean Optics XII*, J. S. Jaffe, ed., Proc. SPIE **2258,** 44–55 (1994).
21. R. M. Pope and E. S. Fry, "Absorption spectrum (380–700 nm) of pure water. II. Integrating cavity measurements," Appl. Opt. **36,** 8710–8723 (1997).
22. R. C. Smith and K. S. Baker, "Optical properties of the clearest natural waters (200–800 nm)," Appl. Opt. **20,** 177–184 (1981).
23. A. H. Barnard, W. S. Pegau, and J. R. V. Zaneveld, "Global relationships of the inherent optical properties of the oceans," J. Geophys. Res. **103,** 24,955–24,968 (1998).
24. M. Sydor and R. A. Arnone, "Effect of suspended particulate and dissolved organic matter on remote sensing of coastal and riverine waters," Appl. Opt. **36,** 6905–6912 (1997).
25. W. M. Balch, P. M. Holligan, S. G. Ackleson, and K. J. Voss, "Biological and optical properties of mesoscale coccolithophore blooms in the Gulf of Maine," Limnol. Oceanogr. **36,** 629–643 (1991).
26. R. A. Maffione and D. R. Dana, "Instruments and methods for measuring the backward-scattering coefficient of ocean waters," Appl. Opt. **36,** 6057–6067 (1997).
27. A. Morel and A. Bricaud, "Theoretical results concerning the optics of phytoplankton, with special reference to remote sensing applications," in *Oceanography from Space*, J. F. R. Gower, ed. (Plenum, New York, 1981), pp. 313–327.
28. C. H. Whitlock, L. R. Poole, and W. M. Houghton, "Spectral scattering properties of turbid waters," Geophys. Res. Lett. **7,** 81–84 (1980).